

Non-Hermitian non-Abelian topological insulators with \mathcal{PT} symmetry

Motohiko Ezawa 

Department of Applied Physics, University of Tokyo, Hongo 7-3-1, 113-8656, Japan

 (Received 18 July 2021; accepted 13 September 2021; published 1 October 2021)

We study a non-Hermitian non-Abelian topological insulator preserving \mathcal{PT} symmetry, where the non-Hermitian term represents nonreciprocal hoppings. As it increases, a spontaneous \mathcal{PT} symmetry breaking transition occurs in the perfect-flat band model from a real-line-gap topological insulator into an imaginary-line-gap topological insulator. By introducing a band bending term, we realize two phase transitions, where a metallic phase emerges between the above two topological insulator phases. We discuss an electric-circuit realization of non-Hermitian non-Abelian topological insulators. We find that the spontaneous \mathcal{PT} symmetry breaking as well as the edge states are well observed by the impedance resonance.

DOI: [10.1103/PhysRevResearch.3.043006](https://doi.org/10.1103/PhysRevResearch.3.043006)

I. INTRODUCTION

Topological insulators are one of the most fascinating ideas in contemporary physics [1,2]. They are characterized by topological numbers such as the winding number, the Chern number, and the \mathbb{Z}_2 index. However, all of these topological numbers are Abelian.

Non-Abelian topological numbers have been discussed in three-band models protected by \mathcal{PT} symmetry [3–7] or C_2T symmetry [8,9]. They were realized in nodal line semimetals [3,4,6,7,10–12] in three dimensions and Weyl points [8] in two dimensions. Non-Abelian topological insulators in one dimension were studied for three-band models [5] and four-band models [13]. They were experimentally observed in photonic systems [6,9], phononic systems [11,14], and transmission lines [5,13]. In addition, a generalization to multiband theories was proposed in nodal line semimetals [3].

Non-Hermitian topological physics have attracted much attention [15–31]. In non-Hermitian systems eigenvalues and eigenfunctions are complex in general. However, they are restricted to be real if \mathcal{PT} symmetry is imposed [15,20,32–36]. There is a \mathcal{PT} symmetry breaking transition, where the eigenvalues and eigenfunctions become complex. Nonreciprocal hopping is such a hopping that the right-going and left-going hopping amplitude are different [37]. It makes a system non-Hermitian. As far as we are aware of, there is no study on non-Hermitian non-Abelian topological phases so far.

In this paper, we study a non-Hermitian non-Abelian topological insulator in an N band model with \mathcal{PT} symmetry. We show that a spontaneous \mathcal{PT} symmetry breaking is induced by increasing the nonreciprocal hoppings from a phase transition

from a real-line-gap topological insulator to an imaginary-line-gap topological insulator in the case of a perfect-flat band model. Furthermore, by introducing a band bending term, we may generalize the model to have a metal with two critical points, where a metallic phase emerges between the above two topological insulator phases. Finally, we show how to implement the present model in electric circuits. The edge states and the spontaneous \mathcal{PT} symmetry breaking are found to be well signaled by the impedance resonance.

II. NON-HERMITIAN NON-ABELIAN TOPOLOGICAL INSULATORS

A. Hermitian Hamiltonian

We start with a Hermitian system capable to describe a non-Abelian topological insulator based of the one-dimensional lattice in Fig. 1(a). We consider generators of $so(N)$ rotation $L_{\alpha\beta}$ indexed by α and β , whose ab components are defined by

$$(L_{\alpha\beta})_{ab} = \delta_{\alpha b} \delta_{\beta a} - \delta_{\alpha a} \delta_{\beta b}. \quad (1)$$

We consider a \mathcal{PT} -invariant Hamiltonian in the momentum space given by [3]

$$H_{\alpha\beta}(k) = R_{\alpha\beta} \left(\frac{k}{2} \right) \text{diag}(\varepsilon_1, \varepsilon_2, \dots, \varepsilon_N) R_{\alpha\beta} \left(\frac{k}{2} \right)^t, \quad (2)$$

where $0 \leq k < 2\pi$, $1 \leq \alpha, \beta \leq N$, $\varepsilon_1, \varepsilon_2, \dots, \varepsilon_N$ are real, and

$$R_{\alpha\beta} \left(\frac{k}{2} \right) = e^{\frac{k}{2} L_{\alpha\beta}} \quad (3)$$

is a rotation matrix given by

$$\begin{aligned} \left[R_{\alpha\beta} \left(\frac{k}{2} \right) \right]_{ab} &= \delta_{ab} + (\delta_{\alpha\alpha} \delta_{b\alpha} + \delta_{\alpha\beta} \delta_{b\beta}) \cos \frac{k}{2} \\ &\quad + (\delta_{\alpha\beta} \delta_{b\alpha} - \delta_{\alpha\alpha} \delta_{b\beta}) \sin \frac{k}{2}. \end{aligned} \quad (4)$$

Published by the American Physical Society under the terms of the Creative Commons Attribution 4.0 International license. Further distribution of this work must maintain attribution to the author(s) and the published article's title, journal citation, and DOI.

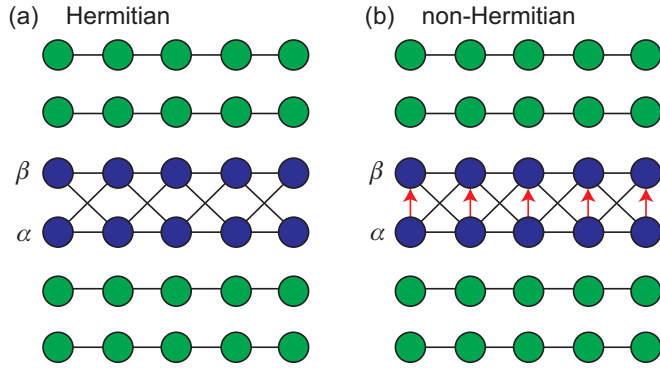


FIG. 1. Illustration of the tight-binding Hamiltonian. (a) Hermitian and (b) non-Hermitian models. Interactions between the α and β chains yield a non-Abelian topological number. All other chains shown in green act as spectators. Red arrows represent nonreciprocal hoppings.

The Hamiltonian (2) is explicitly written as

$$H_{\alpha\beta}(k) = \frac{\varepsilon_\alpha + \varepsilon_\beta}{2} + \frac{\varepsilon_\alpha - \varepsilon_\beta}{2} (\delta_{\alpha\alpha} \delta_{b\alpha} - \delta_{\alpha\beta} \delta_{b\beta}) \cos k + \frac{\varepsilon_\alpha - \varepsilon_\beta}{2} (\delta_{\alpha\beta} \delta_{b\alpha} + \delta_{\alpha\alpha} \delta_{b\beta}) \sin k. \quad (5)$$

It is decomposed into two parts,

$$H_{\alpha\beta}(k) = \bigoplus_{j \neq \alpha, \beta} H_j \oplus H'_{\alpha\beta}(k), \quad (6)$$

where

$$H_j = \varepsilon_j \mathbb{I}_1, \quad (7)$$

and

$$H'_{\alpha\beta}(k) = \left[\frac{\varepsilon_\alpha - \varepsilon_\beta}{2} \begin{pmatrix} \cos k & \sin k \\ \sin k & -\cos k \end{pmatrix} + \frac{\varepsilon_\alpha + \varepsilon_\beta}{2} \mathbb{I}_2 \right]. \quad (8)$$

The Hamiltonian is nontrivial only for the α and β bands, with eigenvalues ε_α and ε_β . All other bands are spectators with respect to the α and β bands. See Fig. 1.

The energy spectrum of the bulk Hamiltonian does not change by the rotation (3) and is given by

$$E(k) = \varepsilon_1, \varepsilon_2, \dots, \varepsilon_N. \quad (9)$$

The eigenfunctions for the 2×2 matrix $H'_{\alpha\beta}(k)$ are

$$\psi_a^+ = \delta_{\alpha\alpha} \sin \frac{k}{2} + \delta_{\alpha\beta} \cos \frac{k}{2}, \quad (10)$$

$$\psi_a^- = -\delta_{\alpha\alpha} \cos \frac{k}{2} + \delta_{\alpha\beta} \sin \frac{k}{2}, \quad (11)$$

while those for H_j are $\psi_a = \delta_{aj}$.

The α and β bands are perfectly flat. They are $(\ell-1)$ -fold degenerate in a finite chain, where ℓ is the number of sites in the chain. See Fig. 2(a1).

Let us review non-Abelian topological numbers for Hermitian systems [3]. The non-Abelian Berry connection or the Berry-Wilczek-Zee (BWZ) connection is defined by

$$A_{\alpha\beta}(k) = \langle \psi_\alpha | \partial_k | \psi_\beta \rangle, \quad (12)$$

while the BWZ phase is defined by

$$\Gamma_{\alpha\beta} = \frac{1}{2\pi} \int_0^{2\pi} A_{\alpha\beta}(k) dk. \quad (13)$$

It is used to define the topological numbers of the system [3].

The eigenfunctions are analytically solved as

$$|\psi_\pm\rangle = \frac{1}{\sqrt{(\psi_1)^2 + (\psi_2)^2}} \{\psi_1, \psi_2\}, \quad (14)$$

$$\psi_1^L = -\gamma_0 \cos k \pm \sqrt{\gamma_0^2 + \xi^2 \sin^2 k}, \quad (15)$$

$$\psi_2^L = -(\gamma_0 + \xi) \sin k. \quad (16)$$

We use these to calculate Eq. (12) as

$$A_{\alpha\beta}(\theta) = -\frac{1}{2} L_{\alpha\beta}. \quad (17)$$

Then, the topological numbers (13) are

$$\Gamma_{\alpha\beta} = -L_{\alpha\beta}/2. \quad (18)$$

All spectator bands are topologically trivial because they are isolated single bands, which remains true even when we make the system non-Hermitian later.

B. \mathcal{PT} Symmetry

We so far considered \mathcal{PT} -symmetric Hermitian systems. In general, the eigenvalues and the eigenvectors are complex in non-Hermitian systems. However, they can be real in the presence of \mathcal{PT} symmetry even in non-Hermitian systems [15,20,32,35]. We review \mathcal{PT} symmetry before we investigate non-Hermitian systems.

We concentrate on nontrivial two bands α and β . We define the parity operator $P = \sigma_z$, whose action is

$$P^{-1} H'_{\alpha\beta}(k) P = H'_{\alpha\beta}(-k). \quad (19)$$

We also define the time-reversal operator $T = \sigma_z K$, with K being the complex-conjugation operator whose action is

$$T^{-1} H'_{\alpha\beta}(k) T = H'^*_{\alpha\beta}(-k). \quad (20)$$

Here, $H'_{\alpha\beta}(\theta)$ has \mathcal{PT} symmetry

$$(\mathcal{PT})^{-1} H'_{\alpha\beta}(k) (\mathcal{PT}) = H'^*_{\alpha\beta}(k), \quad (21)$$

where $\mathcal{PT} = K$.

C. Non-Hermitian Hamiltonian

We generalize the Hermitian non-Abelian system (2) to a non-Hermitian non-Abelian system, keeping \mathcal{PT} symmetry. We consider the Hamiltonian

$$H'_{\alpha\beta}(k; \gamma, \xi) = H'_{\alpha\beta}(k) + i\gamma \sigma_y + \xi \sigma_x \sin k, \quad (22)$$

whose eigenenergies are

$$E'_{\alpha\beta}(k; \gamma, \xi) = \frac{\varepsilon_\alpha + \varepsilon_\beta \pm \sqrt{g(k; \gamma, \xi)}}{2}, \quad (23)$$

with

$$g(k; \gamma, \xi) = (\varepsilon_\alpha - \varepsilon_\beta)^2 - \gamma^2 + 4\xi(\varepsilon_\alpha - \varepsilon_\beta + \xi) \sin^2 k. \quad (24)$$

We explain the meanings of the γ term and the ξ term. The Hamiltonian (22) is Hermitian when $\gamma = 0$. When $\xi = 0$ in

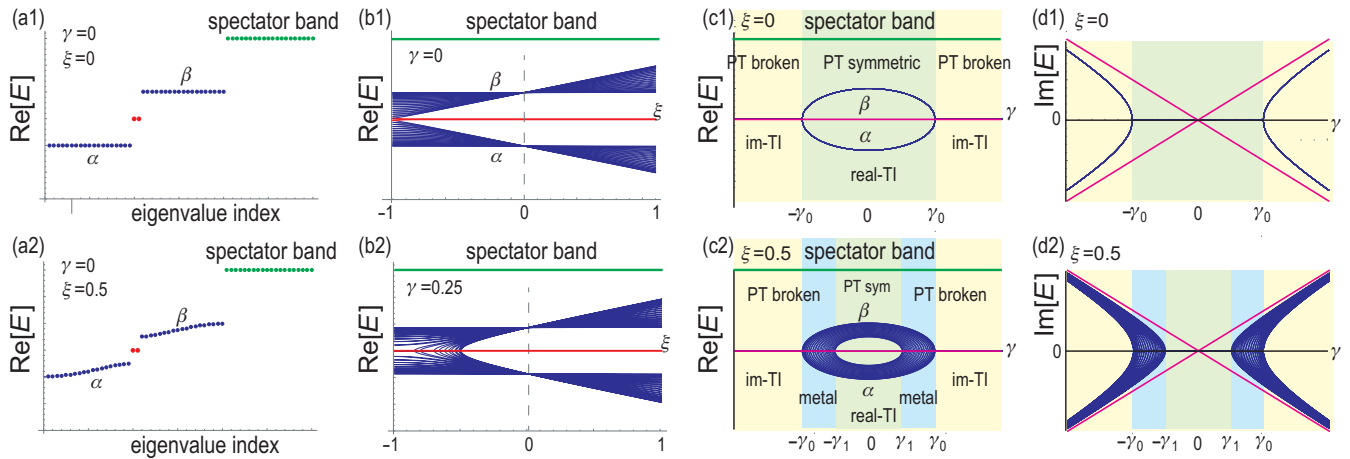


FIG. 2. Energy spectrum of the non-Hermitian Hamiltonian in nanoribbon geometry. Eigenvalues of (a1) the perfectly flat α and β bands with $\xi = 0$ and (a2) the banded bands with $\xi = 0.5$ shown in blue. The red dots represent the topological edge states. The band structure as a function of ξ with (b1) $\gamma = 0$ and (b2) $\gamma = 0.25$. The red lines represent the topological edge states. (c1, c2) Real part of the energy. (d1, d2) Imaginary part of the energy. We set $\xi = 0$ for (c1) and (d1), while we set $\xi = 0.5$ for (c2) and (d2). The bulk bands are colored in blue, while the edge states are colored in red. The spectator band is colored in green. When $\xi = 0$, there are two phases, a real-line-gap topological insulator (real-TI) phase and an imaginary-line-gap topological insulator (im-TI) phase. When $\xi \neq 0$, a metallic phase emerges between these two topological insulator phases. We set $\varepsilon_\alpha = 1$ and $\varepsilon_\beta = 2$.

addition, the band structure is highly degenerate as in Fig. 2 (a1). This degeneracy is resolved by introducing the ξ term as shown in Fig. 2(a2). We show the band structure with $\gamma = 0$ as a function of ξ in Fig. 2(b1). The perfect flat bands at ε_α and ε_β become banded and have dispersions. We also show the band structure with $\gamma = 0.25$ as a function of ξ in Fig. 2(b2).

We illustrate $\text{Re}[E'_{\alpha\beta}(k; \gamma, \xi = 0)]$ in Fig. 2(c1) and $\text{Im}[E'_{\alpha\beta}(k; \gamma, \xi = 0)]$ in Fig. 2(d1) as a function of γ . They are real for $|\gamma| \leq \gamma_0$ with

$$\gamma_0 = \frac{\varepsilon_\alpha - \varepsilon_\beta}{2}, \tag{25}$$

where \mathcal{PT} symmetry is preserved. On the other hand, they are complex for $|\gamma| > \gamma_0$, and hence \mathcal{PT} symmetry is spontaneously broken there. Namely, although the Hamiltonian is \mathcal{PT} -symmetric, eigenvalues and eigenfunctions are no longer real in the spontaneous symmetry broken phase. We show the real and imaginary parts of the energy as a function of γ in Figs. 2(c2) and 2(d2), where the bulk band has a finite width.

We also show the real and imaginary parts of the energy as a function of the momentum k in Fig. 3, where the bands have dispersions.

Specifically, we have

$$E'_{\alpha\beta}\left(\frac{\pi}{2}; \gamma, \xi\right) = \frac{\varepsilon_\alpha + \varepsilon_\beta \pm \sqrt{h(\gamma, \xi)}}{2}, \tag{26}$$

with

$$h(\gamma, \xi) = (\varepsilon_\alpha - \varepsilon_\beta + 2\xi - 2\gamma)(\varepsilon_\alpha - \varepsilon_\beta + 2\xi + 2\gamma). \tag{27}$$

By solving the condition that $E'_{\alpha\beta}(\frac{\pi}{2}; \gamma, \xi)$ is complex, or $h(\gamma, \xi) < 0$, we find a phase transition point γ_1 in addition to the phase transition point γ_0 as

$$\gamma_1 = \frac{\varepsilon_\alpha - \varepsilon_\beta}{2} - \xi = \gamma_0 - \xi. \tag{28}$$

When $\xi > 0$, the bulk energy is real for $|\gamma| \leq \gamma_1$, complex for $|\gamma| > \gamma_1$. On the other hand, when $\xi < 0$, the bulk energy is real for $|\gamma| \leq \gamma_0$, complex for $|\gamma| > \gamma_0$.

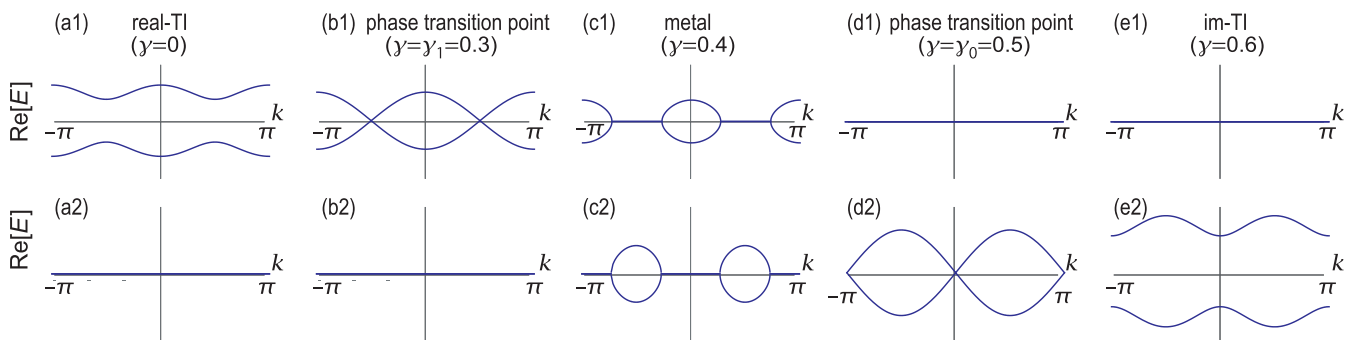


FIG. 3. (a1)–(e1) Real part of the energy and (a2)–(e2) imaginary part of the energy. (a1) and (a2) for a real-line-gap topological insulator (real-TI) with $\gamma = 0$; (b1) and (b2) for a phase transition point with $\gamma = \gamma_1 = 0.3$; (c1) and (c2) for a metal with $\gamma = 0.4$; (d1) and (d2) for a phase transition point with $\gamma = \gamma_0 = 0.5$; (e1) and (e2) for an imaginary-line-gap topological insulator (im-TI) with $\gamma = 0.6$. We set $\xi = 0.2$ for all figures. See also the caption of Fig. 2.

A comment is in order with respect to the skin effect familiar in nonreciprocal systems, where all states are localized at one edge in a finite chain. Such an effect is absent in the present system although it is nonreciprocal. This is because the nonreciprocity is induced by the $i\gamma\sigma_y$ term, representing nonreciprocal hoppings along the y direction as shown by Fig. 1(b). To induce the skin effect, it is necessary to introduce nonreciprocal hoppings along the x direction, but they are prohibited under \mathcal{PT} symmetry.

D. Tight-binding Hamiltonian

The tight-binding Hamiltonian (8) is written in the coordinate space as

$$H'_{\alpha\beta} = H_0 + H_\gamma + H_\xi, \quad (29)$$

with

$$H_0 = \frac{\varepsilon_\alpha - \varepsilon_\beta}{2} \sum_{j=1}^{\ell-1} (|\alpha_j\rangle\langle\alpha_{j+1}| + |\beta_j\rangle\langle\beta_{j+1}| + i|\alpha_j\rangle\langle\beta_{j+1}| - i|\beta_j\rangle\langle\alpha_{j+1}|) + \text{H.c.}, \quad (30)$$

$$H_\gamma = \gamma \sum_{j=1}^{\ell} (|\alpha_j\rangle\langle\beta_j| - |\beta_j\rangle\langle\alpha_j|), \quad (31)$$

$$H_\xi = i\xi \sum_{j=1}^{\ell-1} (|\alpha_j\rangle\langle\beta_{j+1}| - |\beta_j\rangle\langle\alpha_{j+1}|) + \text{H.c.}, \quad (32)$$

where the first two terms in H_0 represent normal hoppings, while the last two terms represent spin-orbit-like imaginary hoppings. The ξ term modifies the spin-orbit-like imaginary hoppings. The γ term represents nonreciprocal hoppings, which make the system non-Hermitian.

The tight-binding Hamiltonians for the spectator bands are simply given by

$$H_{j\neq\alpha,\beta} = \sum_{j=1}^{\ell} \varepsilon_j |j\rangle\langle j| + \sum_{j=1}^{\ell-1} t_j |j\rangle\langle j+1| + \text{H.c.}, \quad (33)$$

where ε_j is the on-site energy and t_j is the hopping parameter.

In this sense, it is enough to consider only the α and β bands for an arbitrary N band system. We illustrate the tight-binding model in Fig. 1.

E. Edge states for non-Hermitian model

We illustrate the tight-binding model (29) in Fig. 1(b). In a finite chain, two localized states emerge at the edges with the energy

$$E(\xi, \gamma) = \frac{\varepsilon_\alpha + \varepsilon_\beta}{2} \pm i\gamma \quad (34)$$

in the presence of the γ term and the ξ term. They are degenerate only in the Hermitian limit ($\gamma = 0$). In contrast to the bulk band, the eigenenergy (34) is complex once γ is introduced even for the \mathcal{PT} symmetric phase. We show Eq. (34) as a function of γ in Fig. 2. In contrast to the bulk band, the eigenenergy (34) has no ξ dependence: See Figs. 2(d1) and 2(d2).

When $\xi = 0$, the eigenfunctions for the edge states $\psi_\alpha(j)$ and $\psi_\beta(j)$ at the j site are perfectly localized at the edges and given by

$$\psi_\alpha(j) = \frac{1}{\sqrt{2}} \delta_{1,j}, \quad \psi_\beta(j) = \frac{-i}{\sqrt{2}} \delta_{1,j}, \quad (35)$$

for the left edge, and

$$\psi_\alpha(j) = \frac{1}{\sqrt{2}} \delta_{\ell,j}, \quad \psi_\beta(j) = \frac{i}{\sqrt{2}} \delta_{\ell,j}, \quad (36)$$

for the right edge. Here, 1 in the subscript of $\delta_{1,j}$ represents the left edge, while ℓ in the subscript of $\delta_{\ell,j}$ represents the right edge. The perfectly localized edge states for $\xi = 0$ are transformed to edge states with finite penetration depth for $\xi \neq 0$.

F. Non-Hermitian non-Abelian topological numbers

We define a non-Hermitian non-Abelian Berry connection or a non-Hermitian BWZ connection by [38]

$$A_{\alpha\beta}^{\text{RL}}(\theta) = \langle \psi_\alpha^{\text{R}} | \partial_\theta | \psi_\beta^{\text{L}} \rangle, \quad (37)$$

where

$$H | \psi_\alpha^{\text{L}} \rangle = \varepsilon_\alpha | \psi_\alpha^{\text{L}} \rangle \quad (38)$$

is the left eigenfunction, and

$$H^\dagger | \psi_\alpha^{\text{R}} \rangle = \varepsilon_\alpha | \psi_\alpha^{\text{R}} \rangle \quad (39)$$

is the right eigenfunction.

We define a non-Hermitian BWZ phase by

$$\Gamma_{\alpha\beta}^{\text{RL}} = \frac{1}{2\pi} \int_0^{2\pi} \text{Re}[A_{\alpha\beta}^{\text{RL}}(\theta)] d\theta, \quad (40)$$

which we use as a non-Hermitian non-Abelian topological number. The eigenfunctions are analytically solved as

$$| \psi_\pm^{\text{L}} \rangle = \frac{1}{\sqrt{(\psi_1^{\text{L}})^2 + (\psi_2^{\text{L}})^2}} \{ \psi_1^{\text{L}}, \psi_2^{\text{L}} \}, \quad (41)$$

$$\psi_1^{\text{L}} = -\gamma_0 \cos k \pm \sqrt{\gamma_0^2 - \gamma^2 + \xi(2\gamma + \xi) \sin^2 k}, \quad (42)$$

$$\psi_2^{\text{L}} = \gamma - (\gamma_0 + \xi) \sin k, \quad (43)$$

and

$$| \psi_\pm^{\text{R}} \rangle = \frac{1}{\sqrt{(\psi_1^{\text{R}})^2 + (\psi_2^{\text{R}})^2}} \{ \psi_1^{\text{R}}, \psi_2^{\text{R}} \}, \quad (44)$$

$$\psi_1^{\text{R}} = \gamma_0 \cos k \pm \sqrt{\gamma_0^2 - \gamma^2 + \xi(2\gamma + \xi) \sin^2 k}, \quad (45)$$

$$\psi_2^{\text{R}} = \gamma + (\gamma_0 + \xi) \sin k. \quad (46)$$

When $\gamma = 0$ and $\xi = 0$, using Eqs. (41) and (44), we calculate the non-Hermitian BWZ connection (37) numerically and find that

$$A_{\alpha\beta}^{\text{RL}} = \frac{1}{2} \begin{pmatrix} 0 & -1 \\ 1 & 0 \end{pmatrix}, \quad (47)$$

which leads to the non-Hermitian BWZ phase (40) as

$$\Gamma_{\alpha\beta}^{\text{RL}} = \frac{1}{2} \begin{pmatrix} 0 & -1 \\ 1 & 0 \end{pmatrix}, \quad (48)$$

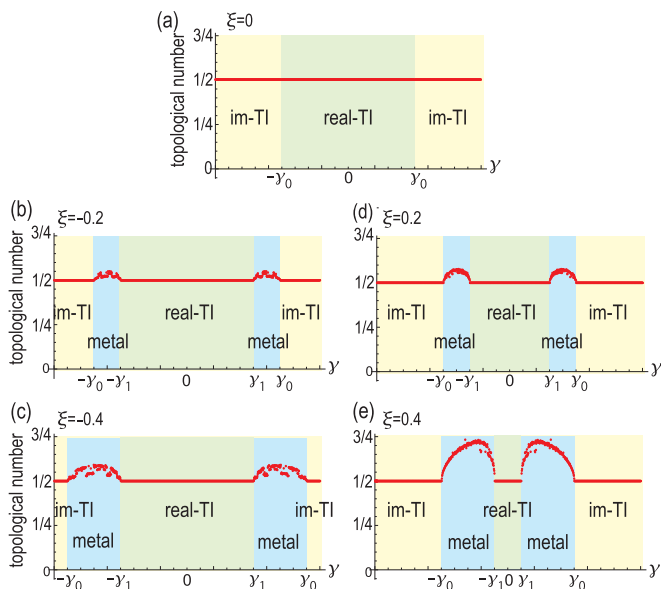


FIG. 4. Non-Abelian topological number marked in red as a function of γ for various ξ . (a) $\xi = 0$, (b) $\xi = -0.2$, (c) $\xi = -0.4$, (d) $\xi = 0.2$, and (e) $\xi = 0.4$. It is quantized at $1/2$ except for the metallic phase. In the figures, real-TI (im-TI) stands for real(imaginary)-line-gap topological insulator phase.

where we explicitly wrote only the nontrivial 2×2 submatrix within the $N \times N$ matrix. Hence, the topological numbers are given by

$$\Gamma_{\alpha\beta}^{\text{RL}} = -\frac{1}{2}L_{\alpha\beta} \quad (49)$$

with Eq. (1). The topological numbers $\Gamma_{\alpha\beta}^{\text{RL}}$ obey essentially the same non-Abelian algebra as $L_{\alpha\beta}$.

When $\gamma \neq 0$ and $\xi = 0$, we calculate the non-Hermitian BWZ connection (37) to find that it is no longer a constant. However, the non-Hermitian BWZ phase (40) is calculated as in Eq. (48), and hence the topological number is quantized as in Eq. (49) for any γ . Nevertheless, the eigenfunctions as well as the eigenvalues are real (i.e., real-line-gap topological insulator phase) only for $\gamma^2 \leq \gamma_0^2$, while the eigenvalues and the eigenfunctions are complex (i.e., imaginary-line-gap topological insulator phase) for $\gamma^2 > \gamma_0^2$. Hence, \mathcal{PT} symmetry is preserved only for $\gamma^2 \leq \gamma_0^2$, and it is spontaneously broken for $\gamma^2 > \gamma_0^2$. The system undergoes a phase transition at $\gamma = \pm\gamma_0$.

When $\gamma \neq 0$ and $\xi \neq 0$, we numerically calculated the topological number (40) with the use of Eqs. (41) and (44). We showed the $(2, 1)$ component of the 2×2 matrix $\Gamma_{\alpha\beta}^{\text{RL}}$ for various values of ξ in Fig. 4. It is quantized to be $1/2$ for $\gamma^2 \leq \gamma_1^2$ and $\gamma^2 > \gamma_0^2$ when $\xi > 0$, while $\gamma^2 \leq \gamma_0^2$ and $\gamma^2 > \gamma_1^2$ when $\xi < 0$, where $\gamma_1 = \gamma_0 - \xi$ as in Eq. (28). On the other hand, it is not quantized for the metallic phase that emerges between γ_0 and γ_1 , as in Fig. 4. It is concluded that the topological numbers are quantized and given by Eq. (49) in the insulator phases.

G. Topological phase diagram

In non-Hermitian systems, there are point-gap insulators and line-gap insulators [27,39] in general. In the point-gap

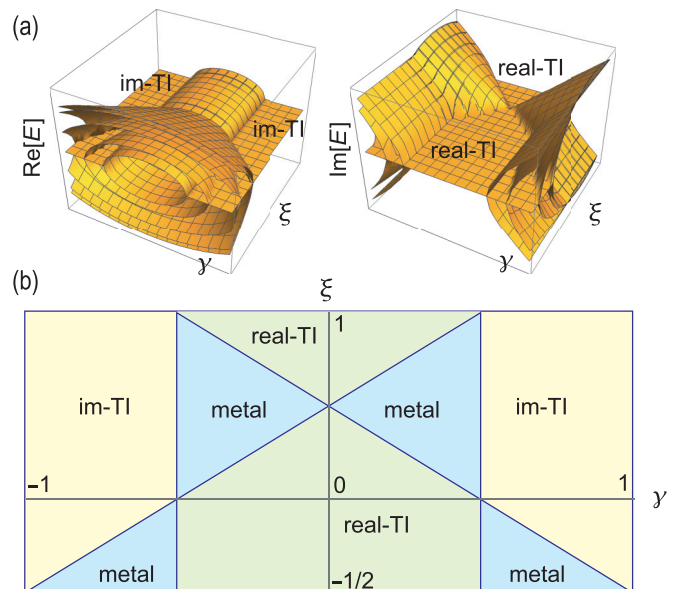


FIG. 5. (a) Real and imaginary parts of the bulk-band energy in the (γ, ξ) plane. (b) Topological phase diagram in the (γ, ξ) plane. Metallic phase appears except for $\xi = 0$. In the figure, real-TI (im-TI) stands for real(imaginary)-line-gap topological insulator phase.

insulator, there is a gap in $|E|$. On the other hand, there are two types of line-gap insulators. A real-line gap topological insulator has a gap in $\text{Re}[E]$, while an imaginary-line-gap topological insulator has a gap in $\text{Im}[E]$. The non-Hermitian metal is such a phase that is neither a real-line-gap insulator nor an imaginary-line-gap insulator nor a point-gap insulator.

We first consider the case $\xi > 0$. For $|\gamma| < \gamma_1$, the system is a non-Hermitian line-gap topological insulator along the $\text{Re}[E]$. The system is metallic for $\gamma_1 \leq |\gamma| \leq \gamma_0$. For $|\gamma| > \gamma_0$, the system is a non-Hermitian line-gap topological insulator along the $\text{Im}[E]$. If $\xi < 0$, the system is a real-line-gap topological insulator for $|\gamma| < \gamma_0$, it is a metal for $\gamma_0 \leq |\gamma| \leq \gamma_1$ and it is an imaginary-line-gap topological insulator for $|\gamma| > \gamma_1$. We show the topological phase diagram in Fig. 5(b). It is consistent with the real and imaginary parts of the energy in the γ - ξ plane as shown in Fig. 5(a).

The real-line-gap topological insulator and the imaginary-line-gap topological insulator are topologically identical because the topological numbers are identical. However, it is obvious that we can differentiate them by a gap position either along the real or imaginary axis.

III. ELECTRIC CIRCUIT SIMULATION

An electric circuit is described by the Kirchhoff current law. By making the Fourier transformation with respect to time, the Kirchhoff current law is expressed as

$$I_a(\omega) = \sum_b J_{ab}(\omega)V_b(\omega), \quad (50)$$

where I_a is the current between node a and the ground, while V_b is the voltage at node b . The matrix $J_{ab}(\omega)$ is called the circuit Laplacian. Once the circuit Laplacian is given, we can uniquely setup the corresponding electric circuit. By equating

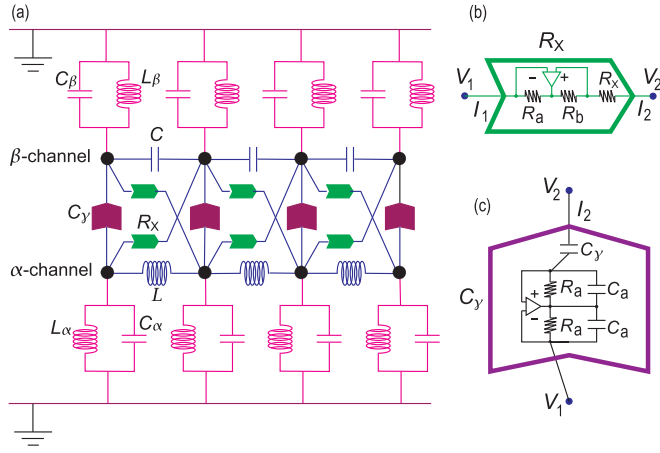


FIG. 6. (a) Illustration of the electric circuit corresponding to the lattice in Fig. 1(b). The hopping along the α -chain (β -chain) is represented by the inductance L (the capacitance C). (b) Negative impedance converter R_X represents an imaginary hopping [40]. (c) Operational amplifier circuit C_Y represents a nonreciprocal hopping [41].

it with the Hamiltonian H as [42,43]

$$J_{ab}(\omega) = i\omega H_{ab}(\omega), \quad (51)$$

it is possible to simulate various topological phases of the Hamiltonian by electric circuits [40–53]. The relations between the parameters in the Hamiltonian and in the electric circuit are determined by this formula.

In the present problem, only the α -chain and the β -chain are active in the tight-binding Hamiltonian as in Fig. 1. Thus, we need only a 2×2 matrix. The circuit Laplacian follows from the Hamiltonian (22) as

$$J'_{\alpha\beta}(k) = i\omega \left[\begin{pmatrix} -\frac{L_\alpha}{\omega^2} \cos k & f_+ \\ f_- & C \cos k \end{pmatrix} + \frac{\varepsilon_\alpha + \varepsilon_\beta}{2} \mathbb{I}_2 \right], \quad (52)$$

with

$$f_\pm = \frac{1}{\omega R_X} (1 + \xi) \sin k \pm \gamma. \quad (53)$$

We may design the electric circuit to realize this circuit Laplacian as in Fig. 6. The main part consists of the α -chain and the β -chain corresponding to the α -chain and the β -chain in the lattice in Fig. 1. Additionally, each node in the i -channel is connected to the ground via a set of inductor L_i and capacitor C_i , where $i = \alpha$ or β to realize the diagonal term $\propto (\varepsilon_\alpha + \varepsilon_\beta)$ in Eq. (52).

Hopping terms along the α -chain and the β -chain are described by the diagonal terms in Eq. (52), where $\pm \cos k = \pm(e^{ik} + e^{-ik})/2$ represents the plus (minus) hopping in the tight-binding model. To simulate the positive and negative hoppings in the Hamiltonian, we replace them with the capacitance $i\omega C$ and the inductance $1/i\omega L$, respectively.

Hopping terms across the α -chain and the β -chain are described by the off-diagonal terms f_\pm in Eq. (52), which consist of two terms proportional to $\sin k$ and γ .

(i) The term proportional to $\sin k$ produces the cross hopping, where $\sin k = (e^{ik} - e^{-ik})/2i$ represents an imaginary hopping in the tight-binding model. The imaginary hopping is

implemented by a negative impedance converter R_X with current inversion [40], as is constructed based on an operational amplifier with resistors: See Fig. 6(b). The voltage-current relation is given by

$$\begin{pmatrix} I_1 \\ I_2 \end{pmatrix} = \frac{1}{R_X} \begin{pmatrix} -\nu & \nu \\ -1 & 1 \end{pmatrix} \begin{pmatrix} V_1 \\ V_2 \end{pmatrix}, \quad (54)$$

with $\nu = R_b/R_a$, where R_X , R_a , and R_b are the resistances in an operational amplifier. We note that the resistors in the operational amplifier circuit are tuned to be $\nu = 1$ in the literature [40] so that the system becomes Hermitian, where the corresponding Hamiltonian represents a spin-orbit interaction. It produces the Hamiltonian

$$H = \frac{1}{\omega R_X} \begin{pmatrix} i & -i \\ i & -i \end{pmatrix} \quad (55)$$

for the Hermitian limit.

(ii) The term $\propto \gamma$ produces the nonreciprocal hopping terms, which are vertical hoppings represented by red arrows in Fig. 1(b). The nonreciprocal hopping is constructed by a combination of an operational amplifier and capacitors [41]

$$\begin{pmatrix} I_{ij} \\ I_{ji} \end{pmatrix} = i\omega C_Y \begin{pmatrix} -1 & 1 \\ -1 & 1 \end{pmatrix} \begin{pmatrix} V_i \\ V_j \end{pmatrix}, \quad (56)$$

as in Fig. 6(c). It corresponds to the Hamiltonian

$$H = C_Y \begin{pmatrix} -1 & 1 \\ -1 & 1 \end{pmatrix}. \quad (57)$$

In this way, the tight-binding Hamiltonian for the present non-Hermitian non-Abelian topological system is implemented in the electric circuit given in Fig. 6.

A. Impedance resonance

The band structure as well as edge states are well observed by impedance resonance, which is defined [42–44] by

$$Z_{ab} = V_a/I_b = G_{ab}, \quad (58)$$

where $G = J^{-1}$ is the Green's function. Taking the nodes $a = b$ at an edge, we show the real and imaginary parts of the impedance for a finite chain as a function of ω in Fig. 7, which are marked in red. For comparison, we also show the impedance for a periodic boundary condition in cyan, where the edge states are absent.

We first study the Hermitian case ($\gamma = 0$) with $\xi = 0$, where the impedance is shown in Figs. 7(a1) and 7(a2). The edge impedance resonance is clear by comparing the periodic boundary condition and the open boundary condition. There are only two bulk peaks in cyan at $\text{Re}[E'_{\alpha\beta}(k; \gamma, \xi)]$. On the other hand, there is an additional peak in red due to the edge states between two bulk peaks, as corresponds to Fig. 2(a1).

Next, we show the impedance for various nonreciprocity γ with $\xi = 0$ in Figs. 7(a1) to 7(f1) and Figs. 7(a2) to 7(f2). The edge impedance resonance rapidly decreases as the increase of γ , as shown in Fig. 7(b1). This is due to the imaginary contribution in Eq. (34). Then, the distance between two bulk peaks becomes narrower, which is consistent with $\text{Re}[E'_{\alpha\beta}(k; \gamma, \xi = 0)]$ as shown in Fig. 2(c1). The two bulk peaks merge into one peak at the spontaneous \mathcal{PT} symmetry breaking point γ_0 , as shown in Fig. 7(e1). The bulk impedance resonance is very

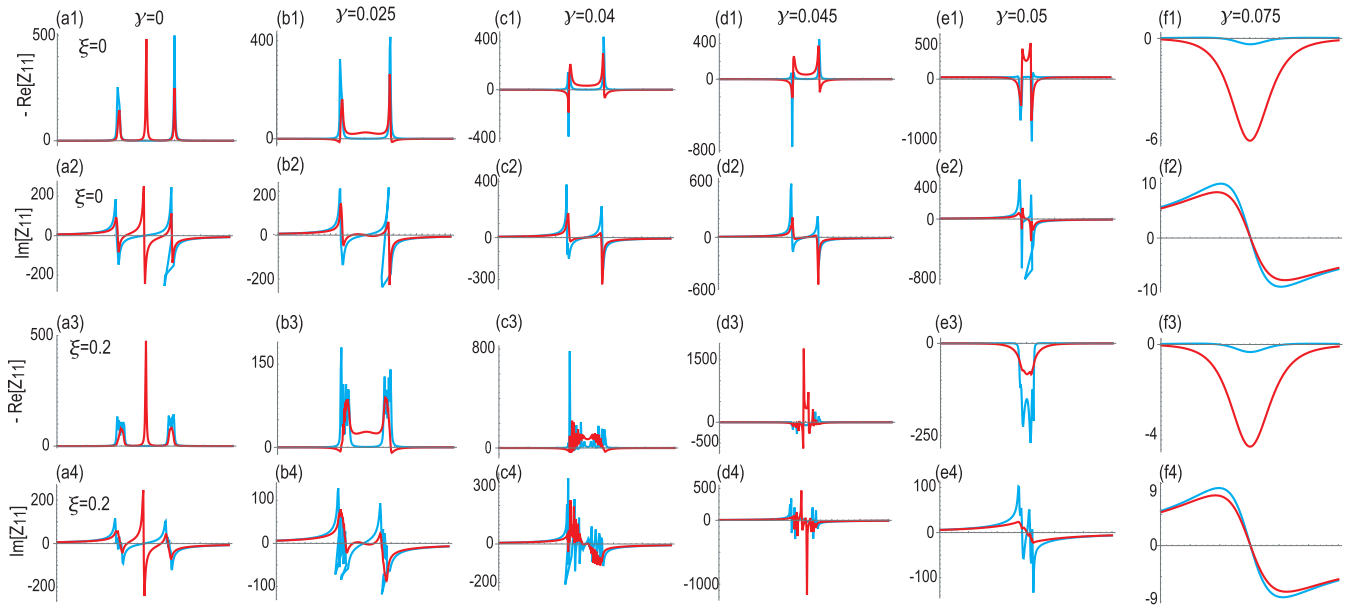


FIG. 7. Real and imaginary parts of impedance Z_{aa} at the edge as a function of frequency ω . (a1)–(a4) Hermitian model with $\gamma = 0$. (b1)–(b4) Non-Hermitian model with $\gamma = 0.025$, (c1)–(c4) with $\gamma = 0.04$ (phase transition point γ_1), (d1)–(d5) with $\gamma = 0.045$, (e1)–(e4) with $\gamma = 0.05$ (phase transition point γ_0), and (f1)–(f4) with $\gamma = 0.075$. We used a finite chain with open boundary condition (red) and periodic boundary condition (cyan). (a1)–(f2) $\xi = 0$. (a3)–(f4) $\xi = 0.2$. We set $\varepsilon_\alpha = 1$ and $\varepsilon_\beta = 1.1$. The length of the chain is 20.

strong due to the gap closing of the bulk band. We also observe the edge impedance resonance in the imaginary-line-gap topological insulating phase, where the impedance resonance is weak comparing to Fig. 7(a1) as shown in Fig. 7(f1). This is also the imaginary contribution in Eq. (34). This phenomenon is understood as follows. The impedance resonance is very sensitive to the eigenvalues of the Hamiltonian. A notable point is that it is suppressed by an imaginary part of the eigenvalue. Since the imaginary component of the eigenvalue is large as in Eq. (34) in imaginary-line-gap insulators, we obtain a small impedance.

We also show the impedance for finite ξ in Figs. 7(a3) to 7(f3) and Figs. 7(a4) to 7(f4), as corresponds to Fig. 2(c2). The bulk impedance peaks become broad, which reflects the broadening of the bulk bands. As a result, the edge impedance peak becomes clearer as in Fig. 7(a3) in comparison to Fig. 7(a1). There are strong cyan resonances at the phase transition point γ_1 point as shown in Figs. 7(c3) and 7(c4). It is due to the gap closing of the bulk band. In Figs. 7(d3) and 7(d4), the impedance structure is complicated, which reflects the metallic band structure. The effect of the ξ term is negligible for the imaginary-line-gap topological phase as shown in Figs. 7(f3) and 7(f4) since the peak of the impedance is broad even for $\xi = 0$ in Figs. 7(f1) and 7(f2). Here, note that ξ appears only in the form of $(1 + \xi)$ in Eq. (53).

IV. CONCLUSION

We proposed a non-Hermitian non-Abelian topological insulator model by imposing \mathcal{PT} symmetry in one dimension. It describes a real-line-gap topological insulator with real eigenvalues in the Hermitian limit. The system undergoes a spontaneous breakdown of \mathcal{PT} symmetry as the non-Hermitian term increases, and turns out to describe an imaginary-line-gap topological insulator, when the bulk bands are perfectly flat. When we introduce a bulk bending term, there are two phase transitions with the emergence of a metal with complex eigenvalues between the above two topological insulators. Finally, we presented how to construct these models in electric circuits. We showed that the spontaneous \mathcal{PT} symmetry breaking as well as topological edge states are well signaled by measuring the frequency dependence of the impedance.

ACKNOWLEDGMENTS

The author is very much grateful to N. Nagaosa for helpful discussions on the subject. This work is supported by the Grants-in-Aid for Scientific Research from MEXT KAKENHI (Grants No. JP17K05490 and No. JP18H03676). This work is also supported by CREST, JST (JPMJCR16F1 and JPMJCR20T2).

- [1] M. Z. Hasan and C. L. Kane, Colloquium: Topological insulators, *Rev. Mod. Phys.* **82**, 3045 (2010).
 [2] X.-L. Qi and S.-C. Zhang, Topological insulators and superconductors, *Rev. Mod. Phys.* **83**, 1057 (2011).

- [3] Q. Wu, A. A. Soluyanov, and T. Bzdusek, Non-Abelian band topology in noninteracting metals, *Science* **365**, 1273 (2019).
 [4] A. Tiwari and T. Bzdušek, Non-Abelian topology of nodal-line rings in \mathcal{PT} -symmetric systems, *Phys. Rev. B* **101**, 195130 (2020).

- [5] Q. Guo, T. Jiang, R.-Y. Zhang, L. Zhang, Z.-Q. Zhang, B. Yang, S. Zhang, and C. T. Chan, Experimental observation of non-Abelian topological charges and edge states, *Nature (London)* **594**, 195 (2021).
- [6] E. Yang, B. Yang, O. You, H.-c. Chan, P. Mao, Q. Guo, S. Ma, L. Xia, D. Fan, Y. Xiang, and S. Zhang, Observation of Non-Abelian Nodal Links in Photonics, *Phys. Rev. Lett.* **125**, 033901 (2020).
- [7] P. M. Lenggenhager, X. Liu, S. S. Tsirkin, T. Neupert, and T. Bzdusek, From triple-point materials to multiband nodal links, *Phys. Rev. B* **103**, L121101 (2021).
- [8] A. Bouhon, Q. Wu, R.-J. Slager, H. Weng, O. V. Yazyev, and T. Bzdusek, Non-Abelian reciprocal braiding of Weyl points and its manifestation in ZrTe, *Nat. Phys.* **16**, 1137 (2020).
- [9] D. Wang, B. Yang, Q. Guo, R.-Y. Zhang, L. Xia, X. Su, W.-J. Chen, J. Han, S. Zhang, and C. T. Chan, Intrinsic in-plane nodal chain and generalized quaternion charge protected nodal link in photonics *Light: Science Applications* **10**, 83 (2021).
- [10] M. Wang, S. Liu, Q. Ma, R.-Y. Zhang, D. Wang, Q. Guo, B. Yang, M. Ke, Z. Liu, and C. T. Chan, Experimental observation of non-Abelian earring nodal links in phononic crystals, [arXiv:2106.06711](https://arxiv.org/abs/2106.06711).
- [11] B. Jiang, A. Bouhon, Z.-K. Lin, X. Zhou, B. Hou, F. Li, R.-J. Slager, and J.-H. Jiang, Experimental observation of non-Abelian topological acoustic semimetals and their phase transitions, *Nature Physics* (2021), doi: 10.1038/s41567-021-01340-x.
- [12] H. Park, S. Wong, X. Zhang, and S. S. Oh, Non-Abelian charged nodal links in dielectric photonic crystal, *ACS Photonics* **8**, 2746 (2021).
- [13] T. Jiang, Q. Guo, R.-Y. Zhang, Z.-Q. Zhang, B. Yang, and C. T. Chan, Four-band non-Abelian topological insulator and its experimental realization, [arXiv:2106.16080](https://arxiv.org/abs/2106.16080).
- [14] B. Peng, A. Bouhon, B. Monserrat, and R.-J. Slager, Non-Abelian braiding of phonons in layered silicates, [arXiv:2105.08733](https://arxiv.org/abs/2105.08733).
- [15] C. M. Bender and S. Boettcher, Real Spectra in Non-Hermitian Hamiltonians Having \mathcal{PT} Symmetry, *Phys. Rev. Lett.* **80**, 5243 (1998).
- [16] C. M. Bender, D. C. Brody, and H. F. Jones, Complex Extension of Quantum Mechanics, *Phys. Rev. Lett.* **89**, 270401 (2002).
- [17] S. Malzard, C. Poli, and H. Schomerus, Topologically Protected Defect States in Open Photonic Systems with Non-Hermitian Charge-Conjugation and Parity-Time Symmetry, *Phys. Rev. Lett.* **115**, 200402 (2015).
- [18] V. V. Konotop, J. Yang, and D. A. Zezyulin, Nonlinear waves in \mathcal{PT} -symmetric systems, *Rev. Mod. Phys.* **88**, 035002 (2016).
- [19] T. Rakovszky, J. K. Asboth, and A. Alberti, Detecting topological invariants in chiral symmetric insulators via losses, *Phys. Rev. B* **95**, 201407(R) (2017).
- [20] R. El-Ganainy, K. G. Makris, M. Khajavikhan, Z. H. Musslimani, S. Rotter, and D. N. Christodoulides, Non-Hermitian physics and \mathcal{PT} symmetry, *Nat. Phys.* **14**, 11 (2018).
- [21] B. Zhu, R. Lu, and S. Chen, \mathcal{PT} symmetry in the non-Hermitian Su-Schrieffer-Heeger model with complex boundary potentials, *Phys. Rev. A* **89**, 062102 (2014).
- [22] S. Yao and Z. Wang, Edge States and Topological Invariants of Non-Hermitian Systems, *Phys. Rev. Lett.* **121**, 086803 (2018).
- [23] L. Jin and Z. Song, Bulk-boundary correspondence in a non-Hermitian system in one dimension with chiral inversion symmetry, *Phys. Rev. B* **99**, 081103(R) (2019).
- [24] S.-D. Liang and G.-Y. Huang, Eigenstate thermalization within isolated spin-chain systems, *Phys. Rev. A* **87**, 012118 (2013).
- [25] D. Leykam, K. Y. Bliokh, Chunli Huang, Y. D. Chong, and Franco Nori, Edge Modes, Degeneracies, and Topological Numbers in Non-Hermitian Systems, *Phys. Rev. Lett.* **118**, 040401 (2017).
- [26] S. Lieu, Topological phases in the non-Hermitian Su-Schrieffer-Heeger model, *Phys. Rev. B* **97**, 045106 (2018).
- [27] Z. Gong, Y. Ashida, K. Kawabata, K. Takasan, S. Higashikawa, and M. Ueda, Topological Phases of Non-Hermitian Systems, *Phys. Rev. X* **8**, 031079 (2018).
- [28] E. Cobanera, A. Alase, G. Ortiz, and L. Viola, Generalization of Bloch's theorem for arbitrary boundary conditions: Interfaces and topological surface band structure, *Phys. Rev. B* **98**, 245423 (2018).
- [29] H. Jiang, C. Yang, and S. Chen, Topological invariants and phase diagrams for one-dimensional two-band non-Hermitian systems without chiral symmetry, *Phys. Rev. A* **98**, 052116 (2018).
- [30] A. Ghatak and T. Das, New topological invariants in non-Hermitian systems, *J. Phys.: Condens. Matter* **31**, 263001 (2019).
- [31] Y. Ashida, Z. Gong, and M. Ueda, Non-Hermitian Physics, *Adv. Phys.* **69**, 3 (2020).
- [32] A. Mostafazadeh, Pseudo-Hermiticity versus \mathcal{PT} symmetry: The necessary condition for the reality of the spectrum of a non-Hermitian Hamiltonian, *J. Math. Phys.* **43**, 205 (2002).
- [33] C. E. Ruter, K. G. Makris, R. El-Ganainy, D. N. Christodoulides, M. Segev, and D. Kip, Observation of parity-time symmetry in optics, *Nat. Phys.* **6**, 192 (2010).
- [34] C. Yuce, Topological phase in a non-Hermitian \mathcal{PT} symmetric system, *Phys. Lett. A* **379**, 1213 (2015).
- [35] L. Feng, R. El-Ganainy, and L. Ge, Non-Hermitian photonics based on parity-time symmetry, *Nat. Photonics* **11**, 752 (2017).
- [36] S. Weimann, M. Kremer, Y. Plotnik, Y. Lumer, S. Nolte, K. G. Makris, M. Segev, M. C. Rechtsman, and A. Szameit, Topologically protected bound states in photonic parity-time-symmetric crystals, *Nat. Mater.* **16**, 433 (2017).
- [37] N. Hatano and D. R. Nelson, Localization Transitions in Non-Hermitian Quantum Mechanics, *Phys. Rev. Lett.* **77**, 570 (1996); Vortex pinning and non-Hermitian quantum mechanics, *Phys. Rev. B* **56**, 8651 (1997); Non-Hermitian delocalization and eigenfunctions, **58**, 8384 (1998).
- [38] F. Wilczek and A. Zee, Appearance of gauge structure in simple dynamical systems, *Phys. Rev. Lett.* **52**, 2111 (1984).
- [39] K. Kawabata, K. Shiozaki, M. Ueda, and M. Sato, Symmetry and Topology in Non-Hermitian Physics, *Phys. Rev. X* **9**, 041015 (2019).
- [40] T. Hofmann, T. Helbig, C. H. Lee, M. Greiter, and R. Thomale, Chiral Voltage Propagation and Calibration in a Topoelectrical Chern Circuit, *Phys. Rev. Lett.* **122**, 247702 (2019).
- [41] T. Helbig, T. Hofmann, S. Imhof, M. Abdelghany, T. Kiessling, L. W. Molenkamp, C. H. Lee, A. Szameit, M. Greiter, and

- R. Thomale, Generalized bulk-boundary correspondence in non-Hermitian topoelectrical circuits, *Nat. Phys.* **16**, 747 (2020).
- [42] S. Imhof, C. Berger, F. Bayer, J. Brehm, L. Molenkamp, T. Kiessling, F. Schindler, C. H. Lee, M. Greiter, T. Neupert, and R. Thomale, Topoelectrical-circuit realization of topological corner modes, *Nat. Phys.* **14**, 925 (2018).
- [43] C. H. Lee, S. Imhof, C. Berger, F. Bayer, J. Brehm, L. W. Molenkamp, T. Kiessling, and R. Thomale, Topoelectrical Circuits, *Commun. Phys.* **1**, 39 (2018).
- [44] T. Helbig, T. Hofmann, C. H. Lee, R. Thomale, S. Imhof, L. W. Molenkamp, and T. Kiessling, Band structure engineering and reconstruction in electric circuit networks, *Phys. Rev. B* **99**, 161114(R) (2019).
- [45] Y. Lu, N. Jia, L. Su, C. Owens, G. Juzeliunas, D. I. Schuster, and J. Simon, Probing the Berry curvature and Fermi arcs of a Weyl circuit, *Phys. Rev. B* **99**, 020302(R) (2019).
- [46] M. Ezawa, Higher-order topological electric circuits and topological corner resonance on the breathing kagome and pyrochlore lattices, *Phys. Rev. B* **98**, 201402(R) (2018).
- [47] M. Ezawa, Non-Hermitian higher-order topological states in nonreciprocal and reciprocal systems with their electric-circuit realization, *Phys. Rev. B* **99**, 201411(R) (2019).
- [48] K. Luo, R. Yu, and H. Weng, Topological nodal states in circuit lattice, *Research* **2018**, 6793752 (2018).
- [49] E. Zhao, Topological circuits of inductors and capacitors, *Ann. Phys.* **399**, 289 (2018).
- [50] M. Ezawa, Non-Hermitian boundary and interface states in nonreciprocal higher-order topological metals and electrical circuits, *Phys. Rev. B* **99**, 121411(R) (2019).
- [51] M. Serra-Garcia, R. Susstrunk, and S. D. Huber, Observation of quadrupole transitions and edge mode topology in an LC circuit network, *Phys. Rev. B* **99**, 020304(R) (2019).
- [52] M. Ezawa, Braiding of Majorana-like corner states in electric circuits and its non-Hermitian generalization, *Phys. Rev. B* **100**, 045407 (2019).
- [53] M. Ezawa, Non-Abelian braiding of Majorana-like edge states and topological quantum computations in electric circuits, *Phys. Rev. B* **102**, 075424 (2020).